Acta Astronautica 132 (2017) 131–142

Contents lists available at ScienceDirect

Acta Astronautica

journal homepage: www.elsevier.com/locate/actaastro

On-orbit identifying the inertia parameters of space robotic systems using simple equivalent dynamics

Wenfu Xu[a,*], Zhonghua Hu[a], Yu Zhang[a], Bin Liang[a,b]

[a] Shenzhen Graduate School, Harbin Institute of Technology, PR China
[b] Department of Automation, Tsinghua University, PR China

ARTICLE INFO

Keywords:
Space robot
Space manipulator
Inertia parameters identification
On-orbit servicing
Simple equivalent dynamics

ABSTRACT

After being launched into space to perform some tasks, the inertia parameters of a space robotic system may change due to fuel consumption, hardware reconfiguration, target capturing, and so on. For precision control and simulation, it is required to identify these parameters on orbit. This paper proposes an effective method for identifying the complete inertia parameters (including the mass, inertia tensor and center of mass position) of a space robotic system. The key to the method is to identify two types of simple dynamics systems: equivalent single-body and two-body systems. For the former, all of the joints are locked into a designed configuration and the thrusters are used for orbital maneuvering. The object function for optimization is defined in terms of acceleration and velocity of the equivalent single body. For the latter, only one joint is unlocked and driven to move along a planned (exiting) trajectory in free-floating mode. The object function is defined based on the linear and angular momentum equations. Then, the parameter identification problems are transformed into non-linear optimization problems. The Particle Swarm Optimization (PSO) algorithm is applied to determine the optimal parameters, i.e. the complete dynamic parameters of the two equivalent systems. By sequentially unlocking the 1st to nth joints (or unlocking the nth to 1st joints), the mass properties of body 0 to n (or n to 0) are completely identified. For the proposed method, only simple dynamics equations are needed for identification. The excitation motion (orbit maneuvering and joint motion) is also easily realized. Moreover, the method does not require prior knowledge of the mass properties of any body. It is general and practical for identifying a space robotic system on-orbit.

1. Introduction

Space robots will play important roles in future space activities such as inspecting, repairing, upgrading and refueling spacecraft [1–5]. They have the potential to extend satellite life, enhance space system capability, decrease operation costs and clean up space debris. Due to dynamic coupling, the motion of a manipulator alters the position and attitude of the base. End-effectors lose the desired target pose (position and attitude) due to the motion of the base [6,7]. This complicates the trajectory planning and control of a space robotic system. Scholars have presented some effective methods for handling the dynamic coupling problem. Umetani and Yoshida presented the generalized Jacobian matrix and resolved the motion control method [8]. Nakamura and Mukherjee [9] used the "bidirectional approach" to plan a path for controlling both the manipulator configuration and spacecraft orientation. Nenchev et al. [10] proposed the reaction null-space control method to address dynamic interaction problems and suppress vibration in the flexible base manipulator. Yoshida et al. [11] addressed the zero reaction maneuver concept and demonstrated it on the ETS-VII. Xu et al. [12] proposed a method based on the particle swarm optimization algorithm to plan the Cartesian point-to-point path of the end-effector and adjust the base attitude simultaneously. Oda et al. [13] proposed a coordinated control method of a space robotic system, simultaneously using the arm controller and the satellite attitude controller. The former estimates the disturbance momentum according to the planned motion of the arm and the current attitude of the base. Then, it sends the results to the satellite controller, which uses the estimated values as feedforward commands to compensate for the reaction of the arm. Angel Flores-Abad et al. [14] proposed an optimal control method of space robots for capturing a tumbling object with uncertainties. Zhu et al. [15,16] proposed a visual servo control framework and corresponding close-loop position-based control strategy for non-cooperative target autonomous capture. The pose and motion of the target is estimated by the extended Kalman filter (EKF). The preceding methods require accurate knowledge of the inertia parameters (mass, inertia tensor, position of center of mass) of each

* Corresponding author.
E-mail addresses: wfxu@hit.edu.cn (W. Xu), hitsz_hzh@163.com (Z. Hu), zy_hitsz@163.com (Y. Zhang), bliang@mail.tsinghua.edu.cn (B. Liang).

http://dx.doi.org/10.1016/j.actaastro.2016.12.031
Received 28 March 2016; Accepted 22 December 2016
Available online 25 December 2016

body. Except for control purpose, these parameters are very important for simulation and analysis on the ground to verify and evaluate the system design, mission planning, tele-operation, and other key issues of space robots. However, these parameters of the system may change on orbit for many reasons, such as fuel consumption, payload deployment, hardware reconfiguration, target capturing, spacecraft docking and mechanical malfunction. Methods are therefore required to identify these dynamic parameters.

For a space robot, whose base is free-floating in 3D space, it has six more degrees of freedoms – three for translation and three for rotation. The dynamic modeling and parameter identification are more challenging. Murotsu [17] proposed two methods for estimating the unknown inertial parameters of manipulated objects. One is based on the linear and angular momentum conservation law. The first method involves measuring the displacements and velocities of the satellite and joints. The second method is based on Newton-Euler equations of motion. Identification methods based on these equations of motion usually use force and torque measurements and identify the target parameters. Yoshida et al. [18] presented a method for identifying the inertia parameters of a free-flying space robot. Using the conservation of momentum laws and considering the effect of gravity gradient torque (unique characteristics in space), the identification algorithm did not require torque or acceleration measurement. However, the mass and centroid position of each body were assumed to be known and not needed to be identified. Lampariello [19] proposed a method for identifying the inertial parameters of a free-flying robot directly on orbit using accelerometers. The method was applied to identify the base body and load on the end-effector, emphasizing the experimental design. In this case, the manipulator parameters were assumed to be known in advance. Abiko and Hirzinger [20] studied online parameter adaptation for momentum control in the post-grasping of a tumbling target with model uncertainty. The proposed adaptation algorithm required measuring the values of the coupling force between the base satellite and robot arm. Only the target's inertia parameters were identified. Ma and Dang [21] presented a robotics-based method for the on-orbit identification of the inertia properties of spacecraft (the base of the space robot), which required accurate kinematics and the dynamic parameters of the manipulator to be known. Thai et al. [22] developed an online momentum-based inertia-parameter identification method for a grasped tumbling target in which the mass properties of the base and manipulator were assumed to be known.

This paper presents a practical and effective approach to identifying the complete inertia parameters of each body of the whole space robotic system, including the base satellite, space manipulator and grasped target. These parameters include the mass, inertia tensor and center of mass position. Only simple dynamics equations are used for inertia parameters identification. The excitation motion is also easily realized. Moreover, no prior knowledge of the mass properties of any system body is required. It is general and practical for on-orbit identifying a space robotic system.

The remainder of this paper is organized as follows. In Section 2, we derive the kinematics and momentum equations of a free-floating space robotic system, establishing the theoretical foundation for inertia parameters identification. In Section 3, we propose an identification method for complete inertial parameters of all bodies based on simple equivalent dynamic models. The identification problem is transformed into non-linear optimization problems. The object functions about the parameters to be determined are correspondingly defined. Section 4 resolves the inertia parameters using the Particle Swarm Optimization (PSO) algorithm. The proposed method is verified in Section 5 based on the simulations of a practical example. The final section presents the summary and conclusion.

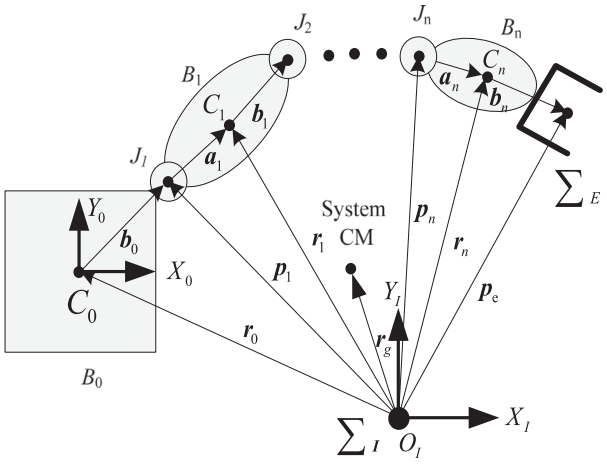

Fig. 1. General model of a serial space robot.

2. Modeling of space robotic system

2.1. Kinematics equations

It is assumed that a space robot is composed of a carrier spacecraft (known as the *Space Base or Base*) and an n-DOFs (degrees of freedom) manipulator (known as the *Space Manipulator*). The space robot captures and services a target satellite (known as the *Target*). The space robotic system can be considered as a serial system composed of n+1 links which are connected by n active joints. The kinematic link of the space robotic system is shown on Fig. 1. Each joint is assumed to have only one DOF. B_0 denotes the satellite main body. B_i (i=1, ..., n) denotes the ith link of the manipulator. J_i is the joint connecting B_{i-1} and B_i. C_i is the position of the center of mass (CM) of B_i.

Some symbols and variables are defined as follows:

$\sum_I$: the inertia frame, also denoted as $\{x_I, y_I, z_I\}$.

$\sum_i$(i=0, ..., n): the body fixed frame of B_i, also denoted as $\{x_i, y_i, z_i\}$; the z_i-axis is the direction of J_i.

${}^i\boldsymbol{A}_j \in \boldsymbol{R}^{3\times3}$: the rotation matrix of $\sum_j$ in relation to $\sum_i$. When $\sum_i$ is the inertia frame, the superscript i can be omitted.

$\boldsymbol{E}$, $\boldsymbol{O}$: the identity matrix and zeros matrix.

m_i, M: m_i ***is the mass of*** $\boldsymbol{B}_i$ and $M = \sum_{i=1}^{n} m_i$.

${}^i\boldsymbol{I}_i \in \boldsymbol{R}^{3\times3}$ (i=0, ..., n): the inertia tensor of B_i in relation to its CM, expressed in $\sum_i$.

$\boldsymbol{k}_i \in \boldsymbol{R}^3$ (i=1, ..., n): the unit vector representing the rotation direction of J_i.

$\boldsymbol{r}_i \in \boldsymbol{R}^3$($i$=1, ..., n): the position vector of C_i.

$\boldsymbol{r}_g \in \boldsymbol{R}^3$: the position vector of the system CM.

$\boldsymbol{p}_i \in \boldsymbol{R}^3$($i$=1, ..., n): the position vector of J_i.

$\boldsymbol{p}_e \in \boldsymbol{R}^3$: the position vector of the end-effector.

$\boldsymbol{a}_i$, $\boldsymbol{b}_i$, $\boldsymbol{l}_i \in \boldsymbol{R}^3$($i$=0, ..., n): the position vectors from J_i to C_i and C_i to J_{i+1}, respectively, and $\boldsymbol{l}_i = \boldsymbol{a}_i + \boldsymbol{b}_i$.

$\boldsymbol{\Theta} \in \boldsymbol{R}^n$: the joint angle vector, i.e., $\boldsymbol{\Theta} = [\boldsymbol{\theta}_1, \ldots, \boldsymbol{\theta}_n]$.

$\boldsymbol{v}_i$, $\boldsymbol{\omega}_i \in \boldsymbol{R}^3$: the linear and angular velocity of B_i.

$\boldsymbol{v}_0$, $\boldsymbol{\omega}_0 \in \boldsymbol{R}^3$: ***the linear and angular velocity of*** B_0.

$\boldsymbol{\Psi}_b \in \boldsymbol{R}^3$: the attitude angle of the base, expressed in terms of z-y-x Euler angles, i.e.

$\boldsymbol{\Psi}_b = [\alpha_b, \beta_b, \gamma_b]^T$.

Based on Fig. 1, the position vectors of the centroid and end-effector of B_i are given respectively as follows:

$$r_i = \boldsymbol{r}_0 + \boldsymbol{b}_0 + \sum_{k=1}^{i-1} (\boldsymbol{a}_k + \boldsymbol{b}_k) + \boldsymbol{a}_i \tag{1}$$

$$\boldsymbol{p}_e = \boldsymbol{r}_0 + \boldsymbol{b}_0 + \sum_{k=1}^{n} (\boldsymbol{a}_k + \boldsymbol{b}_k) \tag{2}$$

The velocities can be obtained by differentiating Eqs. (1) and (2), i.e.,

$$\boldsymbol{v}_i = \dot{\boldsymbol{r}}_i = \boldsymbol{v}_0 + \boldsymbol{\omega}_0 \times (\boldsymbol{r}_i - \boldsymbol{r}_0) + \sum_{k=1}^{i} [\boldsymbol{k}_k \times (\boldsymbol{r}_k - \boldsymbol{p}_k)]\dot{\theta}_k \tag{3}$$

$$\mathrm{v}_\mathrm{e} = \dot{\boldsymbol{p}}_\mathrm{e} = \boldsymbol{v}_0 + \boldsymbol{\omega}_0 \times (\boldsymbol{p}_\mathrm{e} - \boldsymbol{r}_0) + \sum_{k=1}^{n} [\boldsymbol{k}_k \times (\boldsymbol{p}_\mathrm{e} - \boldsymbol{p}_k)]\dot{\theta}_k \tag{4}$$

The angular velocity of the centroid and end-effector of $\mathrm{B}_{\boldsymbol{i}}$ can be derived as follows:

$$\boldsymbol{\omega}_i = \boldsymbol{\omega}_0 + \sum_{k=1}^{i} \boldsymbol{k}_k \dot{\theta}_k \tag{5}$$

$$\boldsymbol{\omega}_\mathrm{e} = \boldsymbol{\omega}_0 + \sum_{k=1}^{n} \boldsymbol{k}_k \dot{\theta}_k \tag{6}$$

Equations and can also be written as follows:

$$\begin{bmatrix} \boldsymbol{v}_\mathrm{e} \\ \boldsymbol{\omega}_\mathrm{e} \end{bmatrix} = \boldsymbol{J}_\mathrm{b} \begin{bmatrix} \boldsymbol{v}_0 \\ \boldsymbol{\omega}_0 \end{bmatrix} + \boldsymbol{J}_\mathrm{m} \dot{\boldsymbol{\Theta}} \tag{7}$$

where $\boldsymbol{J}_\mathrm{b}$ and $\boldsymbol{J}_\mathrm{m}$ are the Jacobian matrices that respectively map the velocities of the base and manipulator to those of the end-effector. They are defined as follows:

$$\boldsymbol{J}_\mathrm{b} = \begin{pmatrix} \boldsymbol{E} & -\boldsymbol{p}_{0\mathrm{e}}^{\times} \\ \boldsymbol{O} & \boldsymbol{E} \end{pmatrix} = \begin{bmatrix} \boldsymbol{J}_\mathrm{bv} \\ \boldsymbol{J}_{b\omega} \end{bmatrix} \tag{8}$$

$$\boldsymbol{J}_\mathrm{m} = \begin{bmatrix} \boldsymbol{k}_1 \times (\boldsymbol{p}_\mathrm{e} - \boldsymbol{p}_1) & \cdots & \boldsymbol{k}_n \times (\boldsymbol{p}_\mathrm{e} - \boldsymbol{p}_n) \\ \boldsymbol{k}_1 & \cdots & \boldsymbol{k}_n \end{bmatrix} = \begin{bmatrix} \boldsymbol{J}_\mathrm{mv} \\ \boldsymbol{J}_{m\omega} \end{bmatrix} \tag{9}$$

$$\boldsymbol{p}_{0e} = \boldsymbol{p}_\mathrm{e} - \boldsymbol{r}_0 \tag{10}$$

In Equations and (9), $\boldsymbol{J}_\mathrm{bv}/\boldsymbol{J}_\mathrm{bw}$ and $\boldsymbol{J}_\mathrm{mv}/\boldsymbol{J}_\mathrm{mw}$ are the sub-matrices of $\boldsymbol{J}_\mathrm{b}$ corresponding to the linear and angular velocities, respectively. $\boldsymbol{p}_{0\mathrm{e}}^{\times}$ is the cross-product operator of $\boldsymbol{p}_{0\mathrm{e}}$.

2.2. Linear and angular momentum equations

For a free-floating space robot, the attitude and orbit of the base are not actively controlled. Since the environment forces and torques on the base are sufficiently small relative to the disturbance torque caused by the manipulator, it is generally assumed that there are no external forces or torques acting upon the space robotic system [8,21,23,24]. As such, the linear and angular momentums of the system are conserved. The conservation equations are written as follows:

$$\boldsymbol{P} = m_0 \boldsymbol{v}_0 + \sum_{i=1}^{n} m_i \dot{\boldsymbol{r}}_i = \boldsymbol{P}_0 \tag{11}$$

$$\boldsymbol{L} = (\boldsymbol{I}_0 \boldsymbol{\omega}_0 + \boldsymbol{r}_0 \times m_0 \dot{\boldsymbol{r}}_0) + \sum_{i=1}^{n} (\boldsymbol{I}_i \boldsymbol{\omega}_i + \boldsymbol{r}_i \times m_i \dot{\boldsymbol{r}}_i) = \boldsymbol{L}_0 \tag{12}$$

where $\boldsymbol{P}$ and $\boldsymbol{L}$ denote the linear and angular momentums, respectively. Their initial values are respectively $\boldsymbol{P}_0$ and $\boldsymbol{L}_0$. Substituting Eqs. (3) and (5) into Eqs. (11) and (12), we obtain the following equations:

$$M\boldsymbol{v}_0 + M(\boldsymbol{r}_{0g}^{\times})^{\mathrm{T}} \boldsymbol{\omega}_0 + \boldsymbol{J}_{Tw} \dot{\boldsymbol{\Theta}} = \boldsymbol{P}_0 \tag{13}$$

$$M\boldsymbol{r}_g^{\times} \boldsymbol{v}_0 + \boldsymbol{I}_w \boldsymbol{\omega}_0 + \boldsymbol{I}_\phi \dot{\boldsymbol{\Theta}} = \boldsymbol{L}_0 \tag{14}$$

Eqs. (13) and (14) can be written in the following matrix form:

$$\begin{pmatrix} M\boldsymbol{E} & M(\boldsymbol{r}_{0g}^{\times})^{\mathrm{T}} \\ M\boldsymbol{r}_\mathrm{g}^{\times} & \boldsymbol{I}_w \end{pmatrix} \begin{bmatrix} \boldsymbol{v}_0 \\ \boldsymbol{\omega}_0 \end{bmatrix} + \begin{bmatrix} \boldsymbol{J}_{Tw} \\ \boldsymbol{I}_\phi \end{bmatrix} \dot{\boldsymbol{\Theta}} = \begin{bmatrix} \boldsymbol{P}_0 \\ \boldsymbol{L}_0 \end{bmatrix} \tag{15}$$

where

$$\boldsymbol{I}_w = \boldsymbol{I}_0 + \sum_{i=1}^{n} (\boldsymbol{I}_i + m_i \boldsymbol{r}_i^{\times} (\boldsymbol{r}_{0i}^{\times})^{\mathrm{T}}) \tag{16}$$

$$\boldsymbol{J}_{Tw} = \sum_{i=1}^{n} (m_i \boldsymbol{J}_{Ti}) \in \boldsymbol{R}^{3\times n} \tag{17}$$

$$\boldsymbol{I}_\phi = \sum_{i=1}^{n} (\boldsymbol{I}_i \boldsymbol{J}_{Ri} + m_i \boldsymbol{r}_i^{\times} \boldsymbol{J}_{Ti}) \tag{18}$$

$$\boldsymbol{J}_{Ti} = [\boldsymbol{z}_1 \times (\boldsymbol{r}_i - \boldsymbol{p}_1), \ldots, \boldsymbol{z}_i \times (\boldsymbol{r}_i - \boldsymbol{p}_i), 0, \ldots, 0] \in \boldsymbol{R}^{3\times n} \tag{19}$$

$$\boldsymbol{J}_{Ri} = [\boldsymbol{z}_1, \ldots, \boldsymbol{z}_i, 0, \ldots, 0] \tag{20}$$

$$\boldsymbol{r}_{0g} = \boldsymbol{r}_g - \boldsymbol{r}_0 \tag{21}$$

$$\mathbf{r}_{0i} = \boldsymbol{r}_i - \boldsymbol{r}_0 \tag{22}$$

Eq. (15) can also be written as follows:

$$\boldsymbol{H}_\mathrm{b} \dot{\boldsymbol{x}}_\mathrm{b} + \boldsymbol{H}_\mathrm{bm} \dot{\boldsymbol{\Theta}} = \boldsymbol{M}_0 \tag{23}$$

Matrices $\boldsymbol{H}_\mathrm{b}$ and $\boldsymbol{H}_\mathrm{bm}$ are the inertia matrix of the base and coupling inertia matrix, respectively. $\mathbf{M}_0$ is the initial momentum. They are defined as follows:

$$\boldsymbol{H}_\mathrm{b} = \begin{pmatrix} M\boldsymbol{E} & M(\boldsymbol{r}_{0g}^{\times})^{\mathrm{T}} \\ M\boldsymbol{r}_g^{\times} & \boldsymbol{I}_w \end{pmatrix} \in \boldsymbol{R}^{6\times 6} \tag{24}$$

$$\boldsymbol{H}_\mathrm{bm} = \begin{bmatrix} \boldsymbol{J}_{Tw} \\ \boldsymbol{I}_\phi \end{bmatrix} \in \boldsymbol{R}^{6\times n} \tag{25}$$

$$\boldsymbol{M}_0 = \begin{bmatrix} \boldsymbol{P}_0 \\ \boldsymbol{L}_0 \end{bmatrix} \in \boldsymbol{R}^{6\times 1} \tag{26}$$

3. Inertia parameter identification method

3.1. Main identification steps

Considering the safety, manipulability, maneuverability and other factors of the space robotic system, we design an ideal configuration for the space manipulator as the standard one. It is the ready and final configuration for most on-orbit operations. It is also used as locking configuration when the manipulator is not needed to be manipulated. This configuration is called normal configuration. The corresponding joint positions are named normal positions. A normal configuration is shown in Fig. 2.

On-orbit identification method of the complete inertia parameter of a space robotic system is presented in the following sections. The key steps are as follows:

3.1.1. Equivalent single-body system identification

The whole system becomes an equivalent single-body system (denoted as $\overline{\mathrm{B}}$) when all of the joints are locked in the normal position,

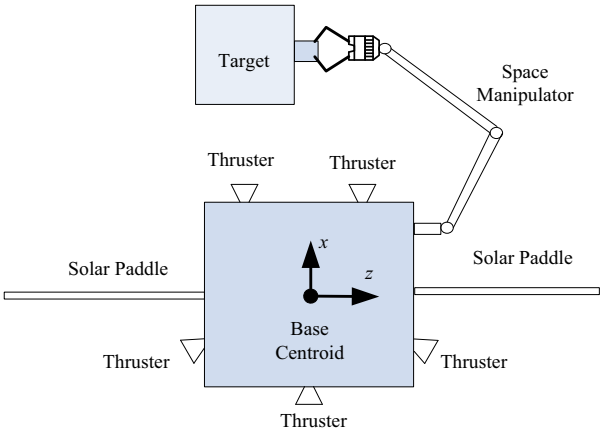

Fig. 2. Normal configuration of the space robotic system.

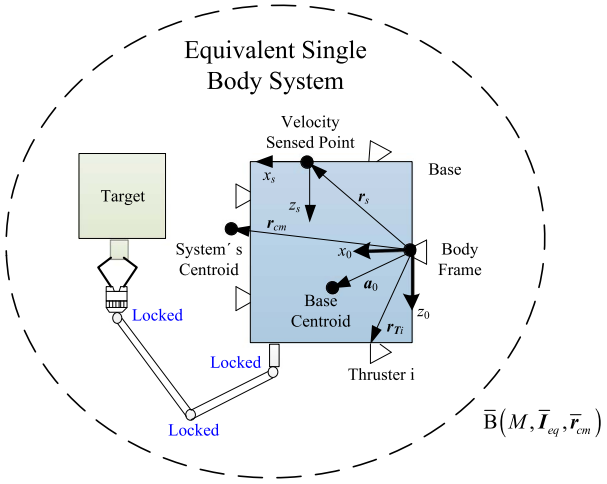

Fig. 3. Equivalent single-body dynamic system.

shown as Fig. 3. The mass, inertia tensor, and the center of mass position of the equivalent single system (i.e. the whole system under the normal configuration) are respectively denoted as M, $\bar{\boldsymbol{I}}_{eq}$ and $\bar{\boldsymbol{r}}_{cm}$.

By maneuvering the equivalent single body and recording the drive forces/torques and the state variables (including the attitude angles, angular velocity and linear acceleration) during the motion, we can identify the inertia parameters of the whole system under the normal configuration. This step is known as "equivalent single-body identification."

3.1.2. Equivalent two-body system identification

When only one joint is unlocked (the other joints are locked into their normal positions), the whole system becomes an equivalent two-body system with one revolute joint. The two bodies are represented as $\tilde{B}_0$ and $\tilde{B}_1$. As an example, the equivalent two-body system formed by unlocking the n^{th} joint is shown in Fig. 4. The inertia parameters of $\tilde{B}_0$ and $\tilde{B}_1$ are denoted as ($\tilde{m}_0$, $\tilde{\boldsymbol{I}}_0$, $\tilde{\boldsymbol{a}}_0$) and ($\tilde{m}_1$, $\tilde{\boldsymbol{I}}_1$, $\tilde{\boldsymbol{a}}_1$). They can be identified by driving the unlocked joint while keeping the other joints locked in the normal position. This is possible when the system mass properties of the total system under the normal configuration are identified. This step is known as "equivalent two-body system identification."

3.1.3. Inertia parameters identification of each body

Combining with the equivalent single-body and two-body dynamic equations, the inertia parameters of $\bar{B}$(i.e.M, $\bar{\boldsymbol{I}}_{eq}$, $\bar{\boldsymbol{r}}_{cm}$), $\tilde{B}_0$(i.e.$\tilde{m}_0$, $\tilde{\boldsymbol{I}}_0$, $\tilde{\boldsymbol{a}}_0$) and $\tilde{B}_1$(i.e.$\tilde{m}_1$, $\tilde{\boldsymbol{I}}_1$, $\tilde{\boldsymbol{a}}_1$) can be identified. By sequentially unlocking the 1st to nth joints, the mass properties of body 0 to n can be identified completely. The process is as follows:

(1) If the 1st joint is unlocked (other joints are locked in the normal positions), $\tilde{B}_0$ is actually the base (i.e. B_0), and $\tilde{B}_1$ is the equivalent body composed of bodies B_1~B_n (denoted as {B_1-B_n}). So, the complete inertial parameters of B_0 and {B_1-B_n} can be identified by unlocking the first joint.

(2) When the 2st joint is unlocked (other joints are locked in the normal positions), $\tilde{B}_0$ is actually the equivalent body composed of B_0-B_1, and $\tilde{B}_1$ is the equivalent body composed of bodies B_2~B_n. The inertia parameters of {B_0-B_1} and {B_2-B_n} can be then identified. Since the parameters of B_0 are identified at the first step, the parameters of B_1 can be then determined.

...

(n) Unlocking the nth joint (other joints are locked in the normal positions), the inertia parameters of {B_0-B_{n-1}} and B_n can be identified using the similar method. When the target is captured and mounted to the end-effector, the mass properties of the target are then determined.

The sequence above may be reversed. That is to say, we can unlock a single joint (other joints are locked in the normal positions) from the order of n to 1.

According to the steps given above, we can see that the key to the method is to identify equivalent single-body and two-body dynamic systems. It should be pointed out that, since the base of the space robot is allowed to move freely in space, all the links move in 3D space, regardless of original n-joint space robotic system, the equivalent single-body system and the equivalent two-body system. In fact, the 3D pose (centroid position and attitude) and motion (linear velocity and angular velocity) of the base are measured to identify all the mass properties of each link (the joint angles and rates are also measured). The details will be given in the following contents.

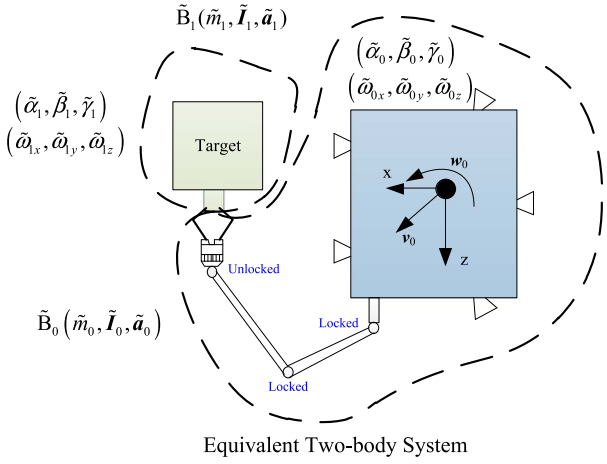

Fig. 4. Equivalent two-body dynamic system.

3.2. Equivalent single-body system identification

The angular momentum of the equivalent single body is calculated as follows:

$$\boldsymbol{H} = \bar{\boldsymbol{I}}_{eq}\boldsymbol{\omega}_0 \tag{27}$$

where $\bar{\mathbf{I}}_{eq}$ is the equivalent inertia tensor of the whole system under the normal configuration. The attitude dynamic equation is obtained by differentiating the two sides of Eq. (27):

$$\bar{\boldsymbol{I}}_{eq}\dot{\boldsymbol{\omega}}_0 + \boldsymbol{\omega} \times \bar{\boldsymbol{I}}_{eq}\boldsymbol{\omega}_0 = \boldsymbol{\tau} \tag{28}$$

When N thrusters are used to control the equivalent single body, the resultant torques are calculated as follows:

$$\boldsymbol{\tau} = \sum_{i=1}^{N} (\boldsymbol{r}_s - \bar{\boldsymbol{r}}_{cm}) \times \boldsymbol{f}_i \tag{29}$$

where $\boldsymbol{f}_i$ is the force generated by the ith thruster; $\mathbf{r}_s$ and $\bar{\mathbf{r}}_{cm}$ are the position vectors of the sensor mounted point and equivalent centroid, respectively, in relation to the base frame $\{x_b, y_b, z_b\}$, as shown in Fig. 3. Substituting Eq. (28) into (29), the following result is obtained:

$$\bar{\boldsymbol{I}}_{eq}\dot{\boldsymbol{\omega}}_0 + \boldsymbol{\omega} \times \bar{\boldsymbol{I}}_{eq}\boldsymbol{\omega}_0 = \sum_{i=1}^{n} (\boldsymbol{r}_s - \bar{\boldsymbol{r}}_{cm}) \times \boldsymbol{f}_i \tag{30}$$

The relationship between the linear velocity (denoted as $\boldsymbol{v}_s$) at the sensor mounted point and that at the equivalent centroid (denoted as $\boldsymbol{v}_{cm}$) is calculated as follows:

$$\boldsymbol{v}_s = \boldsymbol{v}_{cm} + \boldsymbol{\omega} \times (\boldsymbol{r}_s - \bar{\boldsymbol{r}}_{cm}) \tag{31}$$

The following equation is obtained by differentiating (31):

$$\dot{\boldsymbol{v}}_s = \dot{\boldsymbol{v}}_{cm} + \dot{\boldsymbol{\omega}} \times (\boldsymbol{r}_s - \bar{\boldsymbol{r}}_{cm}) + \boldsymbol{\omega} \times [\boldsymbol{\omega} \times (\boldsymbol{r}_s - \bar{\boldsymbol{r}}_{cm})] \tag{32}$$

The linear acceleration of the equivalent centroid can be calculated

according to the resultant force, i.e.,

$$\dot{\boldsymbol{v}}_{\mathrm{cm}} = \sum_{i=1}^{N} \boldsymbol{f}_i / M \tag{33}$$

Combining Eqs. (32) and (33) gives the following equation:

$$M\{\dot{\boldsymbol{\omega}} \times (\boldsymbol{r}_s - \bar{\boldsymbol{r}}_{\mathrm{cm}}) + \boldsymbol{\omega} \times [\boldsymbol{\omega} \times (\boldsymbol{r}_s - \bar{\boldsymbol{r}}_{\mathrm{cm}})]\} = \sum_{i=1}^{N} \boldsymbol{f}_i \tag{34}$$

Eqs. (30) and (34) show that $\bar{\boldsymbol{I}}_{eq}$ cannot be identified if $\boldsymbol{\tau} = \sum_{i=1}^{n} (\boldsymbol{r}_s - \bar{\boldsymbol{r}}_{\mathrm{cm}}) \times \boldsymbol{f}_i$ is 0 and the total mass cannot be identified if $\sum_{i=1}^{n} \boldsymbol{f}_i$ is 0. Therefore, the thrusters should be used to realize the attitude and orbit maneuvering and to identify the complete inertia parameters of the equivalent single body.

It is assumed that the identified mass, inertia tensor and centroid position vectors (expressed in the base frame) are $\hat{M}$, ${}^0\hat{\boldsymbol{I}}_{eq}$ and ${}^0\hat{\mathbf{r}}_{\mathrm{cm}}$ (the left superscript "0" shows that the tensor and the vectors are expressed in 0th frame, i.e. $\sum_0$), respectively. The following relationship should be satisfied:

$$\begin{cases} {}^0\hat{\boldsymbol{I}}_{eq}\,{}^0\dot{\boldsymbol{\omega}}_0 + {}^0\boldsymbol{\omega}_0 \times {}^0\hat{\boldsymbol{I}}_{eq}\,{}^0\boldsymbol{\omega}_0 - \sum_{i=1}^{n} ({}^0\boldsymbol{r}_i - {}^0\hat{\boldsymbol{r}}_{\mathrm{cm}}) \times {}^0\boldsymbol{f}_i \to \boldsymbol{O}_{3\times 1} \\ \hat{M}({}^0\dot{\boldsymbol{v}}_s - {}^0\dot{\boldsymbol{\omega}}_0 \times ({}^0\boldsymbol{r}_s - {}^0\hat{\boldsymbol{r}}_{\mathrm{cm}}) - {}^0\boldsymbol{\omega}_0 \times ({}^0\boldsymbol{\omega}_0 \times ({}^0\boldsymbol{r}_s - {}^0\hat{\boldsymbol{r}}_{\mathrm{cm}})) - \sum_{i=1}^{n} {}^0\boldsymbol{f}_i \\ \quad \to \boldsymbol{O}_{3\times 1} \end{cases} \tag{35}$$

where $\boldsymbol{O}_{3\times 1}$ is a 3×1 zero vector. The left side of (35) is written as follows:

$$\begin{cases} \boldsymbol{P}({}^0\hat{\boldsymbol{I}}_{eq}, {}^0\hat{\boldsymbol{r}}_{\mathrm{cm}}) = {}^0\hat{\boldsymbol{I}}_{eq}\,{}^0\dot{\boldsymbol{\omega}} + {}^0\boldsymbol{\omega} \times {}^0\hat{\boldsymbol{I}}_{eq}\,{}^0\boldsymbol{\omega} - \sum_{i=1}^{n} ({}^0\boldsymbol{r}_i - {}^0\hat{\boldsymbol{r}}_{\mathrm{cm}}) \times {}^0\boldsymbol{f}_i \\ \qquad\qquad = [g_x \quad g_y \quad g_z]^{\mathrm{T}} \\ \boldsymbol{H}(\hat{M}, {}^0\hat{\boldsymbol{r}}_{cm}) = \hat{M}({}^0\dot{\boldsymbol{v}}_s - {}^0\dot{\boldsymbol{\omega}} \times ({}^0\boldsymbol{r}_s - {}^0\hat{\boldsymbol{r}}_{\mathrm{cm}}) - {}^0\boldsymbol{\omega} \times ({}^0\boldsymbol{\omega} \times ({}^0\boldsymbol{r}_s - {}^0\hat{\boldsymbol{r}}_{\mathrm{cm}}))) \\ \qquad\qquad - \sum_{i=1}^{n} {}^0\mathbf{f}_i = [h_x \quad h_y \quad h_z]^{\mathrm{T}} \end{cases} \tag{36}$$

According to Eqs. (35) and (36), the object function for identifying the inertia parameters of the equivalent single body is defined as follows:

$$c(\hat{M}, {}^0\hat{\boldsymbol{I}}_{eq}, {}^0\hat{\boldsymbol{r}}_{\mathrm{cm}}) = \sqrt{g_x^2 + g_y^2 + g_z^2} + \sqrt{h_x^2 + h_y^2 + h_z^2} \tag{37}$$

A certain optimization algorithm can be used to minimize $c(\hat{M}, {}^0\hat{\boldsymbol{I}}_{eq}, {}^0\hat{\boldsymbol{r}}_{\mathrm{cm}})$. When $c(\hat{M}, {}^0\hat{\boldsymbol{I}}_{eq}, {}^0\hat{\boldsymbol{r}}_{\mathrm{cm}}) \to 0$, the parameters $(\hat{M}, {}^0\hat{\boldsymbol{I}}_{eq}, {}^0\hat{\boldsymbol{r}}_{\mathrm{cm}})$ can be used as the identified values.

3.3. Equivalent two-body system identification

As discussed above, an equivalent two-body system is formed when one joint is unlocked and the other joints remain locked. The centroids of the equivalent two bodies (i.e.$\widetilde{\mathrm{B}}_0$ and $\widetilde{\mathrm{B}}_1$) are respectively denoted as $\widetilde{\mathrm{C}}_0$ and $\widetilde{\mathrm{C}}_1$. The base frame $\{x_0y_0z_0\}$ is taken as the body-fixed frame of $\widetilde{\mathrm{B}}_0$ (for the equivalent two-body system, it also denoted as $\{\tilde{x}_0\tilde{y}_0\tilde{z}_0\}$), and $\{\tilde{x}_1\tilde{y}_1\tilde{z}_1\}$ is the body-fixed frame of $\widetilde{\mathrm{B}}_1$. If the ith joint is unlocked, $\{x_iy_iz_i\}$ is taken as $\{\tilde{x}_2\tilde{y}_2\tilde{z}_2\}$. The link lengths ${}^0\tilde{\mathbf{l}}_0$ and ${}^1\tilde{\mathbf{l}}_1$ are known. The rotation matrix between the two frames above is denoted as ${}^i\widetilde{\boldsymbol{A}}_j$. The position vectors of $\widetilde{\mathrm{C}}_0$ and $\widetilde{\mathrm{C}}_1$ in relation to the body-fixed frame are ${}^0\tilde{\boldsymbol{a}}_0$ and ${}^1\tilde{\boldsymbol{a}}_1$, respectively (Fig. 5).

3.3.1. Motion equations

The following velocity relationships are easily derived:

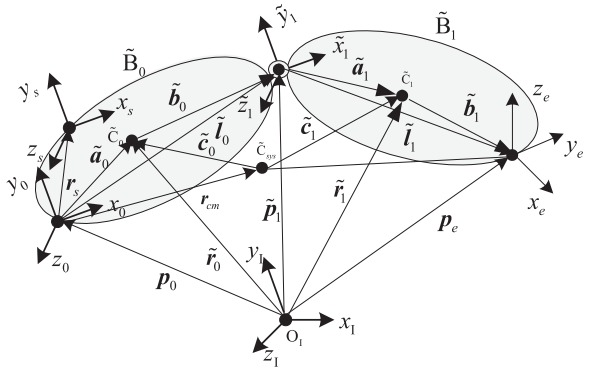

Fig. 5. Kinematic relationship of the equivalent two-body system.

$$\begin{cases} \tilde{\boldsymbol{v}}_0 = \boldsymbol{v}_s + \boldsymbol{\omega}_0 \times \boldsymbol{A}_0({}^0\tilde{\boldsymbol{a}}_0 - {}^0\boldsymbol{r}_s) \\ \tilde{\boldsymbol{v}}_1 = \boldsymbol{v}_s + \boldsymbol{\omega}_0 \times \boldsymbol{A}_0\left({}^0\tilde{\boldsymbol{l}}_0 - {}^0\boldsymbol{r}_s\right) + \tilde{\boldsymbol{\omega}}_1 \times (\boldsymbol{A}_1{}^1\tilde{\boldsymbol{a}}_1) \\ \tilde{\boldsymbol{\omega}}_1 = \boldsymbol{\omega}_0 + \boldsymbol{k}_i\dot{\theta}_i \end{cases} \tag{38}$$

The centroid positions of the two bodies in relation to the inertia frame are as follows:

$$\tilde{\boldsymbol{r}}_0 = \tilde{\boldsymbol{p}}_0 + \boldsymbol{A}_0\,{}^0\tilde{\boldsymbol{a}}_0 \tag{39}$$

$$\tilde{\boldsymbol{r}}_1 = \tilde{\boldsymbol{p}}_0 + \boldsymbol{A}_0\,{}^0\tilde{\boldsymbol{l}}_0 + \boldsymbol{A}_1{}^1\tilde{\boldsymbol{a}}_1 \tag{40}$$

The following relationship is formed:

$$\tilde{m}_0\tilde{\boldsymbol{r}}_0 + \tilde{m}_1\tilde{\boldsymbol{r}}_1 = M\boldsymbol{r}_g \tag{41}$$

where $\tilde{m}_0$ and $\tilde{m}_1$ are the masses of $\widetilde{\mathrm{B}}_0$ and $\widetilde{\mathrm{B}}_1$, respectively. According to (39)–(41), we obtain the following:

$$\tilde{\boldsymbol{p}}_0 = \frac{M\boldsymbol{r}_g - \tilde{m}_1\boldsymbol{A}_0\,{}^0\tilde{\boldsymbol{a}}_0 - \tilde{m}_2\left(\boldsymbol{A}_0\,{}^0\tilde{\boldsymbol{l}}_0 + \boldsymbol{A}_1{}^1\tilde{\boldsymbol{a}}_1\right)}{\tilde{m}_1 + \tilde{m}_2} \tag{42}$$

Substituting Eq. (42) into Eqs. (39) and (40) gives the function expressions of $\tilde{\boldsymbol{r}}_0$ and $\tilde{\boldsymbol{r}}_1$ in relation to ${}^0\tilde{\boldsymbol{a}}_0$ and ${}^1\tilde{\boldsymbol{a}}_1$.

However, under the normal configuration, ${}^0\tilde{\boldsymbol{a}}_0$ and ${}^1\tilde{\boldsymbol{a}}_1$, and the centroid of the equivalent single-body system ${}^0\bar{\boldsymbol{r}}_{cm}$ satisfy the following equation:

$$\tilde{m}_0\,{}^0\tilde{\boldsymbol{a}}_0 + \tilde{m}_1\left({}^0\tilde{\boldsymbol{l}}_0 + {}^0\widetilde{\boldsymbol{A}}_1\,{}^1\tilde{\mathbf{a}}_1\right) = M\,{}^0\bar{\mathbf{r}}_{cm} \tag{43}$$

where ${}^0\widetilde{\boldsymbol{A}}_1$ is the attitude matrix of frame$\{\tilde{x}_1\tilde{y}_1\tilde{z}_1\}$ in relation to frame $\{\tilde{x}_0\tilde{y}_0\tilde{z}_0\}$ under the normal configuration.

The relationship of the inertia tensors of $\widetilde{\mathrm{B}}_0$, $\widetilde{\mathrm{B}}_1$ and the equivalent single-body system under the normal configuration can then be derived.

According to the parallel axis theorem, the following relationship is formed:

$$\begin{aligned} {}^0\bar{\boldsymbol{I}}_{eq} = {}^0\widetilde{\boldsymbol{I}}_0 + \tilde{m}_0[({}^0\tilde{\boldsymbol{c}}_0^{\mathrm{T}0}\tilde{\boldsymbol{c}}_0)\boldsymbol{E} - {}^0\tilde{\boldsymbol{c}}_0\,{}^0\tilde{\boldsymbol{c}}_0^{\mathrm{T}}] + {}^0\widetilde{\boldsymbol{A}}_1\,{}^1\widetilde{\boldsymbol{I}}_1\left({}^0\widetilde{\boldsymbol{A}}_1\right)^{\mathrm{T}} \\ + \tilde{m}_1[({}^0\tilde{\boldsymbol{c}}_1^{\mathrm{T}0}\tilde{\boldsymbol{c}}_1)\boldsymbol{E} - {}^0\tilde{\mathbf{c}}_1\,{}^0\tilde{\mathbf{c}}_1^{\mathrm{T}}] \end{aligned} \tag{44}$$

where

$$\begin{cases} {}^0\tilde{\boldsymbol{c}}_0 = {}^0\tilde{\boldsymbol{a}}_0 - {}^0\bar{\boldsymbol{r}}_{\mathrm{cm}} \\ {}^0\tilde{\boldsymbol{c}}_1 = {}^0\tilde{\boldsymbol{l}} + {}^0\widetilde{\boldsymbol{A}}_1\,{}^1\tilde{\boldsymbol{a}}_1 - {}^0\bar{\boldsymbol{r}}_{\mathrm{cm}} \end{cases} \tag{45}$$

Moreover, the masses of $\widetilde{\mathrm{B}}_0$, $\widetilde{\mathrm{B}}_1$ and the equivalent single-body system meet the following relationship:

$$\tilde{m}_0 + \tilde{m}_1 = M \tag{46}$$

Eqs. (43), (44) and (46) reveal that the inertia parameters of one body can be expressed as the functions of those of the other body, based on the identified parameters of the equivalent single-body system.

3.3.2. Object function for parameter identification

The linear and angular momentum equations of the two-body system are calculated as follows:

$$\boldsymbol{P} = \widetilde{m}_0\tilde{\boldsymbol{v}}_0 + \widetilde{m}_1\tilde{\boldsymbol{v}}_1 \tag{47}$$

$$\boldsymbol{H} = \left(\boldsymbol{A}_0\,{}^0\tilde{\boldsymbol{I}}_0\boldsymbol{A}_0^{\mathrm{T}}\right)\boldsymbol{\omega}_0 + \left(\widetilde{\boldsymbol{A}}_1\,{}^1\tilde{\boldsymbol{I}}_1\widetilde{\boldsymbol{A}}_1^{\mathrm{T}}\right)\widetilde{\boldsymbol{\omega}}_1 + \tilde{\boldsymbol{r}}_0 \times (\widetilde{m}_0\tilde{\boldsymbol{v}}_0) + \tilde{\boldsymbol{r}}_1 \times (\widetilde{m}_1\tilde{\boldsymbol{v}}_1) \tag{48}$$

Because no external forces or torques act on the free-floating system, the linear and angular momentums are conserved. Assuming that their initial values are 0, the conservation equations are given as follows:

$$\begin{cases} \boldsymbol{P} = \widetilde{m}_0\tilde{\boldsymbol{v}}_0 + \widetilde{m}_1\tilde{\boldsymbol{v}}_1 = \boldsymbol{O} \\ \boldsymbol{H} = \left(\boldsymbol{A}_0\,{}^0\tilde{\boldsymbol{I}}_0\boldsymbol{A}_0^{\mathrm{T}}\right)\boldsymbol{\omega}_0 + \left(\widetilde{\boldsymbol{A}}_1\,{}^1\tilde{\boldsymbol{I}}_1\widetilde{\boldsymbol{A}}_1^{\mathrm{T}}\right)\widetilde{\boldsymbol{\omega}}_1 + \tilde{\boldsymbol{r}}_0 \times (\widetilde{m}_0\tilde{\boldsymbol{v}}_0) + \tilde{\boldsymbol{r}}_1 \times (\widetilde{m}_1\tilde{\boldsymbol{v}}_1) = \boldsymbol{O} \end{cases} \tag{49}$$

The left side of Eq. (49) is written as the function of the inertia parameters of the 0th body, i.e., $\widetilde{\mathrm{B}}_0$:

$$\boldsymbol{P}(\widetilde{m}_0, {}^0\tilde{\boldsymbol{a}}_0) = \hat{m}_1\tilde{\boldsymbol{r}}_1 + \hat{m}_1\tilde{\boldsymbol{r}}_2 = [g_x \quad g_y \quad g_z]^{\mathrm{T}} \tag{50}$$

$$\begin{aligned} \boldsymbol{H}(\widetilde{m}_0, {}^0\tilde{\boldsymbol{I}}_0, {}^0\tilde{\boldsymbol{a}}_0) = &\left(\boldsymbol{A}_0\,{}^0\tilde{\boldsymbol{I}}_0\boldsymbol{A}_0^{\mathrm{T}}\right)\boldsymbol{\omega}_0 + \left(\widetilde{\boldsymbol{A}}_1\,{}^1\tilde{\boldsymbol{I}}_1\widetilde{\boldsymbol{A}}_1^{\mathrm{T}}\right)\widetilde{\boldsymbol{\omega}}_1 + \tilde{\boldsymbol{r}}_0 \times (\widetilde{m}_0\tilde{\boldsymbol{v}}_0) \\ &+ \tilde{\boldsymbol{r}}_1 \times (\widetilde{m}_1\tilde{\boldsymbol{v}}_1) = [h_x \quad h_y \quad h_z]^{\mathrm{T}} \end{aligned} \tag{51}$$

The object function for identifying the inertia parameters of the equivalent two-body system is defined as follows:

$$c(\widetilde{m}_0, {}^0\tilde{\mathbf{I}}_0, {}^0\tilde{\mathbf{a}}_0) = \sqrt{g_x^2 + g_y^2 + g_z^2} + \sqrt{h_x^2 + h_y^2 + h_z^2} \tag{52}$$

A certain optimization algorithm can be used to minimize $c(\widetilde{m}_0, {}^0\tilde{\boldsymbol{I}}_0, {}^0\tilde{\boldsymbol{a}}_0)$. When $c(\widetilde{m}_0, {}^0\tilde{\boldsymbol{I}}_0, {}^0\tilde{\boldsymbol{a}}_0) \to 0$, the parameters $(\widetilde{m}_0, {}^0\tilde{\boldsymbol{I}}_0, {}^0\tilde{\boldsymbol{a}}_0)$ are identified. The parameters $(\widetilde{m}_1, {}^1\tilde{\boldsymbol{I}}_1, {}^1\tilde{\boldsymbol{a}}_1)$ are then calculated according to Eqs. (43), (44) and (46). Therefore, the complete inertia parameters of the two-body system are identified.

4. Parameters resolving based on the optimization algorithm

Based on the preceding derivation, the inertia parameter identification problems for equivalent single- and two-body systems are transformed into non-linear optimization problems. The object functions are respectively defined as Eqs. (37) and (52). Considering the advantages of the Particle Swarm Optimization (PSO) algorithm [25] for solving unconstrained nonlinear problems, we apply the PSO algorithm in this paper.

In a particle swarm optimizer, instead of using genetic operators, the individuals are "evolved" by cooperation and competition between the individuals themselves through generations. Each individual is known as a "particle" and adjusts its flying according to its own flying experience and that of its companions. This represents a potential solution to a problem and is treated as a point in a D-dimensional space. The i^{th} particle is described as follows:

$$\boldsymbol{X}_i = (x_{i1}, x_{i2}, \ldots, x_{iD}) \tag{53}$$

The best previous position (the position giving the best fitness value) of any particle is recorded and represented as follows:

$$\boldsymbol{P}_i = (p_{i1}, p_{i2}, \ldots, p_{iD}) \tag{54}$$

The best particle out of all of the particles in the population is denoted by:

$$\boldsymbol{P}_g = (p_{g1}, p_{g2}, \ldots, p_{gD}) \tag{55}$$

The velocity of particle i is

$$\boldsymbol{V}_i = (v_{i1}, v_{i2}, \ldots, v_{iD}) \tag{56}$$

The particles are manipulated according to the following equations:

$$v_{id} = wv_{id} + c_1\mathrm{rand}()(p_{id} - x_{id}) + c_2\mathrm{Rand}()(p_{gd} - x_{id}) \tag{57}$$

$$x_{id} = x_{id} + v_{id} \tag{58}$$

where rand() and Rand() are two random functions in the range [0,1]; c_1 and c_2 are two positive constants known as the cognitive and social parameters, respectively. The weight coefficient w balances the local and global searches. It behaves as a positive constant or even a positive linear/nonlinear function of time. The particle swarm optimizer has been found to be robust and fast in solving nonlinear, non-differentiable and multi-modal problems.

The inertia tensor and centroid position vector are expressed as follows:

$${}^0\bar{\boldsymbol{I}}_{eq} = \begin{bmatrix} \bar{I}_{eq,xx} & \bar{I}_{eq,xy} & \bar{I}_{eq,xz} \\ \bar{I}_{eq,xy} & \bar{I}_{eq,yy} & \bar{I}_{eq,yz} \\ \bar{I}_{eq,xz} & \bar{I}_{eq,yz} & \bar{I}_{eq,zz} \end{bmatrix}, \quad {}^0\bar{\boldsymbol{r}}_{\mathrm{cm}} = \begin{bmatrix} \bar{r}_x \\ \bar{r}_y \\ \bar{r}_z \end{bmatrix} \tag{59}$$

$${}^0\tilde{\boldsymbol{I}}_0 = \begin{bmatrix} \tilde{I}_{0,xx} & \tilde{I}_{0,xy} & \tilde{I}_{0,xz} \\ \tilde{I}_{0,xy} & \tilde{I}_{0,yy} & \tilde{I}_{0,yz} \\ \tilde{I}_{0,xz} & \tilde{I}_{0,yz} & \tilde{I}_{0,zz} \end{bmatrix}, \quad {}^0\tilde{\boldsymbol{a}}_0 = \begin{bmatrix} \tilde{a}_{0x} \\ \tilde{a}_{0y} \\ \tilde{a}_{0z} \end{bmatrix} \tag{60}$$

The parameter sets for the equivalent single- and two-body systems are defined as follows:

$$\boldsymbol{X}_{\mathrm{single}} = (M, \bar{I}_{eq,xx}, \bar{I}_{eq,yy}, \bar{I}_{eq,zz}, \bar{I}_{eq,xy}, \bar{I}_{eq,xz}, \bar{I}_{eq,yz}, \bar{r}_x, \bar{r}_y, \bar{r}_z) \in \boldsymbol{R}^{10} \tag{61}$$

$$\boldsymbol{X}_{\mathrm{two}} = (\widetilde{m}_0, \tilde{I}_{0,xx}, \tilde{I}_{0,yy}, \tilde{I}_{0,zz}, \tilde{I}_{0,xy}, \tilde{I}_{0,xz}, \tilde{I}_{0,yz}, \tilde{a}_{0x}, \tilde{a}_{0y}, \tilde{a}_{0z}) \in \boldsymbol{R}^{10} \tag{62}$$

The population size is assumed to be n_p and the maximum number of iterations to train is N_{max}. The iteration number is denoted by k. The optimization procedure is similar to that adopted in [12].

5. Simulation study

5.1. A space robot with six joints

The space robotic system studied in the paper is shown as Fig. 6. It is composed of a carrier spacecraft (called *Space Base* or *Base*) and a 6R manipulator (called *Space Manipulator*). The frames fixed on the multi-body system are defined as Fig. 7 (when the joint angles are all zeros), where Z_i is the direction of J_i. Table 1 lists the dimensions and mass properties of the bodies (*Sat* and B_i stand for the satellite and the

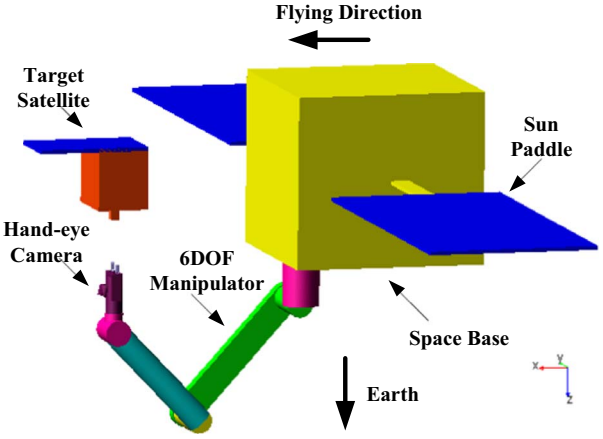

Fig. 6. The space robotic system studied in the paper.

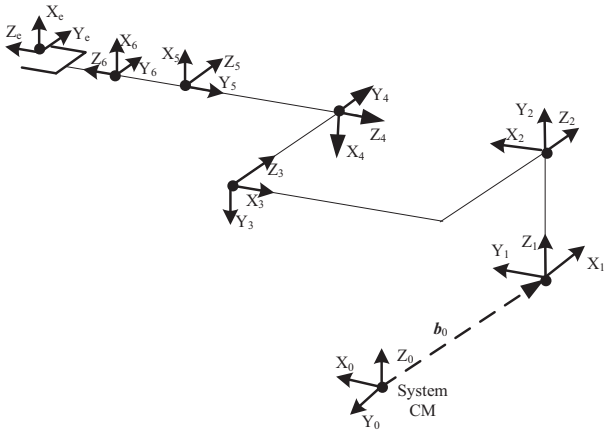

Fig. 7. The body-fixed frames of the space robotic system.

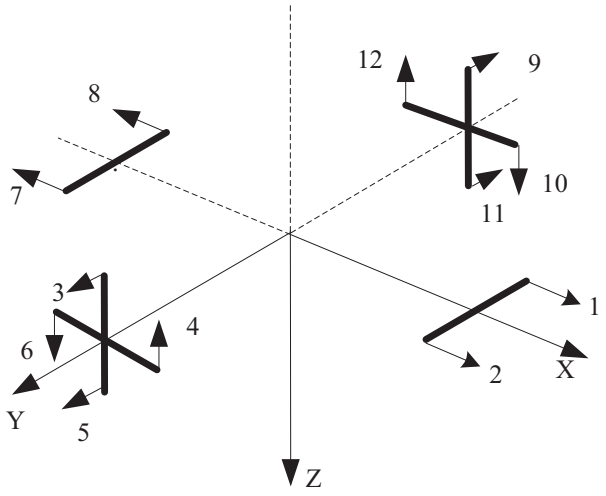

Fig. 8. Arrangement of the jet propulsion system.

ith body, respectively). The vectors ${}^{i}\boldsymbol{a}_i$, ${}^{i}\boldsymbol{b}_i$ and ${}^{i}\boldsymbol{I}_i$ are expressed in $\sum_i$. In the following sections, the origin of the inertia frame is the system' CM, i.e. $\boldsymbol{r}_g=\boldsymbol{O}$.

5.2. Thruster layout

It is assumed that there are 12 thrusters mounted on the base. To realize the 6-DOF attitude and orbit control, the thrusters are arranged as shown in Fig. 8. The directions denoted by the arrows are those of the jet vectors. The directions of the generated forces are opposite to those of the arrows. The normal amplitudes of the thrusters are 2N. Table 2 lists the installation positions and thrust vectors of the jet thrusters.

5.3. Identification results of the equivalent mass properties

We create the dynamic model using co-simulation platform based on ADAMS and Simulink software to verify the proposed inertia parameter identification methods. In order to verify the principle of the proposed method from a theoretical point of view, the measurement errors are not considered in the simulation.

For the equivalent single body, the 12 thrusters are used sequentially for orbital maneuvering. The working time of each thruster is $t_1 = 5s$. The total time is $t_f = 12t_1 = 60s$.Table 3 shows the orbital maneuvering process. The attitude angles, angular velocity, linear acceleration and linear velocity are recorded at each sample time. PSO algorithms are then applied to these data to determine the optimal inertia parameters. Fig. 9 shows the global best value of cost function versus the iteration number from the simulation results. The global best value decreases monotonously and even crosses a wide and nearly unchangeable region. The findings indicate that the PSO algorithm has formidable power in searching for the optimal parameters. Table 4 shows the theoretic and identified parameters. It should be pointed out that only three valid digits are retained. We can see that, the identification accuracy is very high. The results are used in the equivalent two-body system identification.

5.4. Identification results of each bodies

For the equivalent two-body system identification, the base is free floating, i.e., its attitude and orbit are not actively controlled. Only one joint is unlocked and driven to generate the movement.

The first joint is driven to move from the normal position (denoted as 0°) to +30° and −30° and then back to the normal position. The mean speed is 2°/s. Table 5 lists the motion nodes. The third spline functions are used to plan the joint trajectory under the sample time Δt=0.1 s. The planned trajectory is used for the ADAMS model. The attitude angular and linear velocity of the base and the angle and angular velocity of the joint are recorded during the simulation. The PSO algorithm is then applied to the data to determine the inertia parameters of the equivalent two-body system.

Using the method proposed above, the complete inertia parameters of all the bodies are identified. Limited by the length of the paper, we only give part results here. The global best value of the cost function versus the iteration number for identifying $\widetilde{B}_0$ and $\widetilde{B}_1$ is shown in Fig. 10. The global best value decreases monotonously, indicating that the PSO algorithm has been searching the optimal parameters. When the first joint is the unlocked joint, $\widetilde{B}_0$ is actually B_0 and $\widetilde{B}_1$ is actually the equivalent body composed of the links of the space manipulator,

Table 1
The mass properties of the space robotic system.

		Sat	B_1	B_2	B_3	B_4	B_5	B_6 (Including the target)
Mass (kg)		400	12	10	10	8	6	30
${}^{i}\boldsymbol{a}_i$(m)		0	0	0.270	0	0	0	−0.270
		0	0	0	0	0	−0.034	0
		0	0.150	−0.251	0.150	−0.350	0	0.430
${}^{i}\boldsymbol{b}_i$(m)		0.357	0	0.560	0	0	0	0
		−0.010	0	0	0	0	−0.066	0
		0.419	0.150	−0.049	0.150	−0.700	0	0
${}^{i}\boldsymbol{I}_i$ (kg m^2)	Ixx	30	0.510	0.278	0.420	0.500	0.330	2.398
	Iyy	28	0.510	1.811	0.420	0.500	0.172	2.678
	Izz	32	0.200	1.690	0.150	0.210	0.260	1.405
	Ixy	0.260	0	0	0	0	0	−0.069
	Ixz	0.370	0	0.263	0	0	0	0.013
	Iyz	−0.290	0	0	0	0	0	0.051

Table 2
Installation positions and thrust vectors of the jet thrusters.

Thruster i	Installation position $\boldsymbol{r}_i$ (m)	Force vector	Thruster i	Installation position $\boldsymbol{r}_i$ (m)	Force vector
1	[−0.7, −0.2, 0]	[−1,0,0]	7	[0, 0.2, 0]	[0,1]
2	[−0.7, 0.2, 0]	[−1,0,0]	8	[0, −0.2, 0]	[0,1]
3	[−0.35, 0.35, −0.2]	[0,−1,0]	9	[0.35, −0.35, 0.2]	[−1,0,0]
4	[−0.55, 0.35, 0]	[0,0,−1]	10	[−0.55, −0.35, 0]	[0,0,−1]
5	[0.35, 0.35, 0.2]	[0,−1,0]	11	[0.35, −0.35, 0.2]	[0,1,0]
6	[0.15, 0.35, 0]	[0,0,−1]	12	[0.15, −0.35, 0]	[0,0,1]

Table 3
Orbital maneuvering using jet thrusters.

Maneuver number	Thruster used (N)	Working time (s)	Maneuver number	Thruster used (N)	Working time (s)
1	$\boldsymbol{f}_1$	$0 \le t < t_1$	7	$\boldsymbol{f}_4$	$6t_1 \le t < 7t_1$
2	$\boldsymbol{f}_7$	$t_1 \le t < 2t_1$	8	$\boldsymbol{f}_{12}$	$7t_1 \le t < 8t_1$
3	$\boldsymbol{f}_2$	$2t_1 \le t < 3t_1$	9	$\boldsymbol{f}_5$	$8t_1 \le t < 9t_1$
4	$\boldsymbol{f}_8$	$3t_1 \le t < 4t_1$	10	$\boldsymbol{f}_9$	$9t_1 \le t < 10t_1$
5	$\boldsymbol{f}_3$	$4t_1 \le t < 5t_1$	11	$\boldsymbol{f}_6$	$10t_1 \le t < 11t_1$
6	$\boldsymbol{f}_{11}$	$5t_1 \le t < 6t_1$	12	$\boldsymbol{f}_{10}$	$11t_1 \le t < 12t_1$

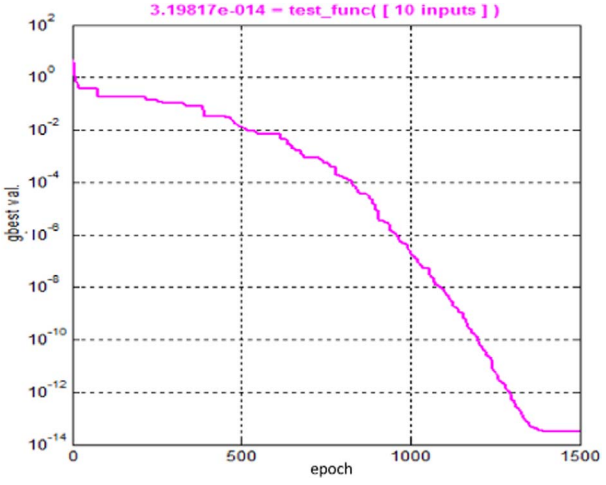

Fig. 9. Variation of the global best fitness for equivalent single-body identification.

Table 4
Theoretic and identified parameters of the equivalent single body.

Parameters	Theoretic value x	Identification value $\hat{x}$	Identification error $\lvert x-\hat{x}\rvert$ ($\lvert x-\hat{x}\rvert/\lvert x\rvert$)
M (kg)	476	475.999	$2.2\times10^{-13}(4.62\times10^{-14}\%)$
$\bar{I}_{eq,xx}$ (kg m^2)	65.460	65.460	$4.3\times10^{-14}(6.57\times10^{-14}\%)$
$\bar{I}_{eq,yy}$ (kg m^2)	93.997	93.997	$3.1\times10^{-15}(3.29\times10^{-15}\%)$
$\bar{I}_{eq,zz}$ (kg m^2)	66.931	66.931	$1.0\times10^{-14}(1.49\times10^{-14}\%)$
$\bar{I}_{eq,xy}$ (kg m^2)	−2.111	−2.111	$2.8\times10^{-14}(1.33\times10^{-12}\%)$
$\bar{I}_{eq,xz}$ (kg m^2)	−25.195	−25.195	$3.5\times10^{-14}(1.39\times10^{-13}\%)$
$\bar{I}_{eq,yz}$ (kg m^2)	−3.741	−3.741	$2.66\times10^{-12}(7.11\times10^{-11}\%)$
$\bar{r}_x$ (m)	0.103	0.103	$9.0\times10^{-15}(8.73\times10^{-12}\%)$
$\bar{r}_y$ (m)	0.007	0.007	$1.7\times10^{-14}(2.43\times10^{-10}\%)$
$\bar{r}_z$ (m)	0.078	0.078	$4.2\times10^{-14}(5.38\times10^{-11}\%)$

which is locked in the normal configuration. The inertia parameters of {B_1-B_n} are correspondingly identified sequentially by unlocking the other joints. The identified parameters of each bodies are shown in Tables 6–12. The theoretic, identified values and the errors are also listed. We can see that the identification accuracy is very high. That is to say, the proposed method is very simple and effective.

Table 5
Motion nodes of the first joint.

Node number	Joint angle (deg)	Time (s)	Node number	Joint angle (deg)	Time (s)
0	0	0	5	−15	37.5
1	15	7.5	6	−30	45
2	30	15	7	−15	52.5
3	15	22.5	8	0	60

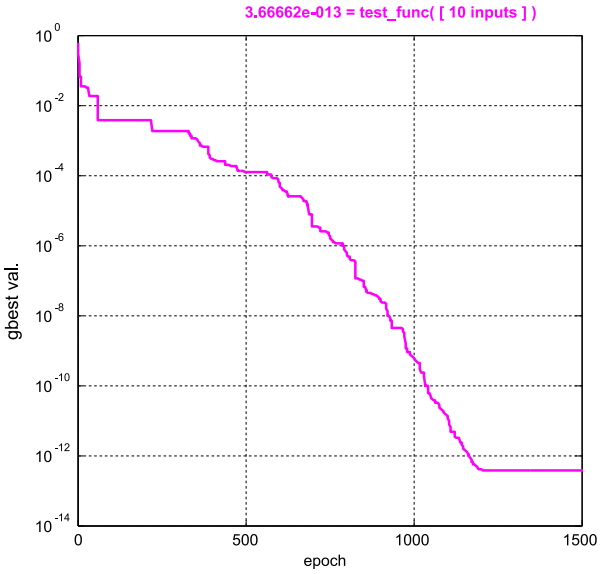

Fig. 10. Variation of the global best fitness for identifying b6 based on equivalent two-body identification.

Table 6
Theoretic and identified parameters of B_0.

Parameters	Theoretic value x	Identification value $\hat{x}$	Identification error $\lvert x-\hat{x}\rvert$ ($\lvert x-\hat{x}\rvert/\lvert x\rvert$)
m_0 (kg)	400	399.9415	0.0585(0.015%)
$I_{0,xx}$ (kg m^2)	30	30.117	0.117(0.39%)
$I_{0,yy}$ (kg m^2)	28	28.109	0.109(0.39%)
$I_{0,zz}$ (kg m^2)	32	31.993	0.007(0.022%)
$I_{0,xy}$ (kg m^2)	0.260	0.259	0.001(0.38%)
$I_{0,xz}$ (kg m^2)	0.370	0.335	0.035(9.5%)
$I_{0,yz}$ (kg m^2)	−0.290	−0.289	0.001(0.34%)
a_{0x} (m)	0	-5.22×10^{-5}	5.22×10^{-5}(/)
a_{0y} (m)	0	1.39×10^{-6}	1.39×10^{-6}(/)
a_{0z} (m)	0	2×10^{-4}	2×10^{-4}(/)

5.5. Error analysis of the identified dynamics

In order to analyze the effect of the identified parameters on the dynamic system, we respectively assign normal (ideal) parameters and

Table 7
Theoretic and identified parameters of B_1.

Parameters	Theoretic value x	Identification value $\hat{x}$	Identification error $\|x-\hat{x}\|$ ($\|x-\hat{x}\|/\|x\|$)
m_1(kg)	12	12.010	0.010(0.083%)
$I_{1,xx}$(kg m^2)	0.510	0.523	0.013(2.5%)
$I_{1,yy}$(kg m^2)	0.510	0.519	0.009(1.8%)
$I_{1,zz}$(kg m^2)	0.200	0.196	0.004(2%)
$I_{1,xy}$(kg m^2)	0	9.1×10^{-11}	9.1×10^{-11}(/)
$I_{1,xz}$(kg m^2)	0	6.0×10^{-4}	6.0×10^{-4}(/)
$I_{1,yz}$(kg m^2)	0	-6.36×10^{-9}	6.36×10^{-9}(/)
a_{1x}(m)	0	3.0×10^{-4}	3.0×10^{-4}(/)
a_{1y}(m)	0	-1.8×10^{-14}	1.8×10^{-14}(/)
a_{1z}(m)	0.150	0.140	0.010(6.7%)

Table 8
Theoretic and identified parameters of B_2.

Parameters	Theoretic value$x$	Identification value$\hat{x}$	Identification error $\|x-\hat{x}\|$ ($\|x-\hat{x}\|/\|x\|$)
m_2(kg)	10	9.966	0.034(0.34%)
$I_{2,xx}$(kg m^2)	0.278	0.285	0.007(2.5%)
$I_{2,yy}$(kg m^2)	1.811	1.817	0.006(0.32%)
$I_{2,zz}$(kg m^2)	1.690	1.689	0.001(0.059%)
$I_{2,xy}$(kg m^2)	0	9.41×10^{-9}	9.41×10^{-9}(/)
$I_{2,xz}$(kg m^2)	0.263	0.257	0.006(2.3%)
$I_{2,yz}$(kg m^2)	0	5.1×10^{-11}	5.1×10^{-11}(/)
a_{2x}(m)	0.270	0.272	0.002(0.74%)
a_{2y}(m)	0	-1.30×10^{-13}	1.30×10^{-13}(/)
a_{2z}(m)	−0.251	−0.252	0.001(0.39%)

Table 9
Theoretic and identified parameters of B_3.

Parameters	Theoretic value x	Identification value $\hat{x}$	Identification error $\|x-\hat{x}\|$ ($\|x-\hat{x}\|/\|x\|$)
m_3(kg)	10	10.007	0.007(0.07%)
$I_{3,xx}$(kg m^2)	0.420	0.414	0.006(1.4%)
$I_{3,yy}$(kg m^2)	0.420	0.404	0.016(3.8%)
$I_{3,zz}$(kg m^2)	0.150	0.141	0.009(6.0%)
$I_{3,xy}$(kg m^2)	0	8.8×10^{-13}	8.8×10^{-13}(/)
$I_{3,xz}$(kg m^2)	0	8.0×10^{-4}	8.0×10^{-4}(/)
$I_{3,yz}$(kg m^2)	0	-6.5×10^{-13}	-6.5×10^{-13}(/)
a_{3x}(m)	0	-5.0×10^{-4}	5.0×10^{-4}(/)
a_{3y}(m)	0	3.0×10^{-15}	3.0×10^{-15}(/)
a_{3z}(m)	0.150	0.149	0.001(0.067%)

Table 10
Theoretic and identified parameters of B_4.

Parameters	Theoretic value x	Identification value $\hat{x}$	Identification error $\|x-\hat{x}\|$ ($\|x-\hat{x}\|/\|x\|$)
m_4(kg)	8	7.908	0.092(1.2%)
$I_{4,xx}$(kg m^2)	0.500	0.509	0.009(1.8%)
$I_{4,yy}$(kg m^2)	0.500	0.501	0.001(0.2%)
$I_{4,zz}$(kg m^2)	0.210	0.218	0.008(3.8%)
$I_{4,xy}$(kg m^2)	0	6.5×10^{-13}	6.5×10^{-13}(/)
$I_{4,xz}$(kg m^2)	0	-4.7×10^{-13}	4.7×10^{-13}(/)
$I_{4,yz}$(kg m^2)	0	1.4×10^{-10}	-1.4×10^{-10}(/)
a_{4x}(m)	0	1.0×10^{-15}	1.0×10^{-15}(/)
a_{4y}(m)	0	1.4×10^{-8}	1.4×10^{-8}(/)
a_{4z}(m)	−0.350	−0.346	0.004(1.1%)

Table 11
Theoretic and identified parameters of B_5.

Parameters	Theoretic value x	Identification value $\hat{x}$	Identification error $\|x-\hat{x}\|$ ($\|x-\hat{x}\|/\|x\|$)
m_5(kg)	6	6.069	0.069(1.2%)
$I_{5,xx}$(kg m^2)	0.330	0.323	0.007(2.1%)
$I_{5,yy}$(kg m^2)	0.172	0.164	0.008(4.6%)
$I_{5,zz}$(kg m^2)	0.260	0.261	0.001(0.38%)
$I_{5,xy}$(kg m^2)	0	-1.8×10^{-13}	1.8×10^{-13}(/)
$I_{5,xz}$(kg m^2)	0	-4.6×10^{-14}	4.6×10^{-14}(/)
$I_{5,yz}$(kg m^2)	0	3.7×10^{-9}	3.7×10^{-9}(/)
a_{5x}(m)	0	-4.0×10^{-15}	4.0×10^{-15}(/)
a_{5y}(m)	−0.034	−0.033	0.001(2.9%)
a_{5z}(m)	0	-1.9×10^{-8}	1.9×10^{-8}(/)

Table 12
Theoretic and identified parameters of B_6.

Parameters	Theoretic value x	Identification value $\hat{x}$	Identification error $\|x-\hat{x}\|$ ($\|x-\hat{x}\|/\|x\|$)
m_6(kg)	30	30.009	0.009(0.03%)
$I_{6,xx}$(kg m^2)	2.398	2.395	0.003(0.13%)
$I_{6,yy}$(kg m^2)	2.678	2.676	0.002(0.11%)
$I_{6,zz}$(kg m^2)	1.405	1.405	6.8×10^{-4}(0.048%)
$I_{6,xy}$(kg m^2)	−0.069	−0.068	5.0×10^{-14}(7.2×10^{-11}%)
$I_{6,xz}$(kg m^2)	0.013	0.014	0.001(7.7%)
$I_{6,yz}$(kg m^2)	0.051	0.051	2.0×10^{-15}(7.4×10^{-13}%)
a_{6x}(m)	−0.270	−0.270	8.4×10^{-5}(3.1×10^{-4}%)
a_{6y}(m)	0	-2.2×10^{-8}	2.2×10^{-8}(/)
a_{6z}(m)	0.430	0.429	0.01(2.3%)

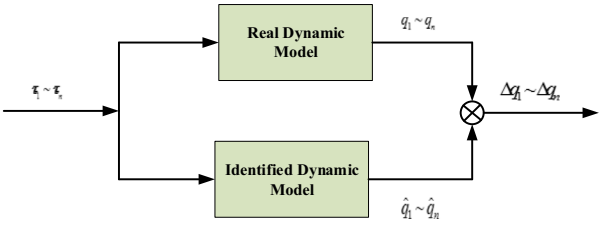

Fig. 11. Error analysis chart under the same driving torques.

identified parameters to the dynamic systems created in Adams. The corresponding models are called “Real Dynamic Model” and “Identified Dynamic Model”. Then, the same drive torques are used to drive the two models. Through comparing the output of the system state, including the pose of the base and the joint angles of the manipulator, we can analyze the difference of the two models. The concept is shown as Fig. 11.

The drive torque of each joint is set as $\tau_i=A_i\ \sin(\omega_i t+\varphi_i)$ and simulation time length is 2 s. The parameters ω_i and φ_i are shown in Table 13.

According to the simulation results, the error curves of the pose of the base (centroid position and attitude) and each joint of the manipulator are shown in Fig. 12 and Fig. 13. The maximum values

Table 13
The parameters of driving torques of each joint.

ith torque	τ_1	τ_2	τ_3	τ_4	τ_5	τ_6
A_i	1.5	−1.2	1.0	0.15	−0.1	0.05
ω_i	4π	3π	2π	2π	3π	4π
φ_i	0	0.5π	π	1.5π	−0.5π	−π

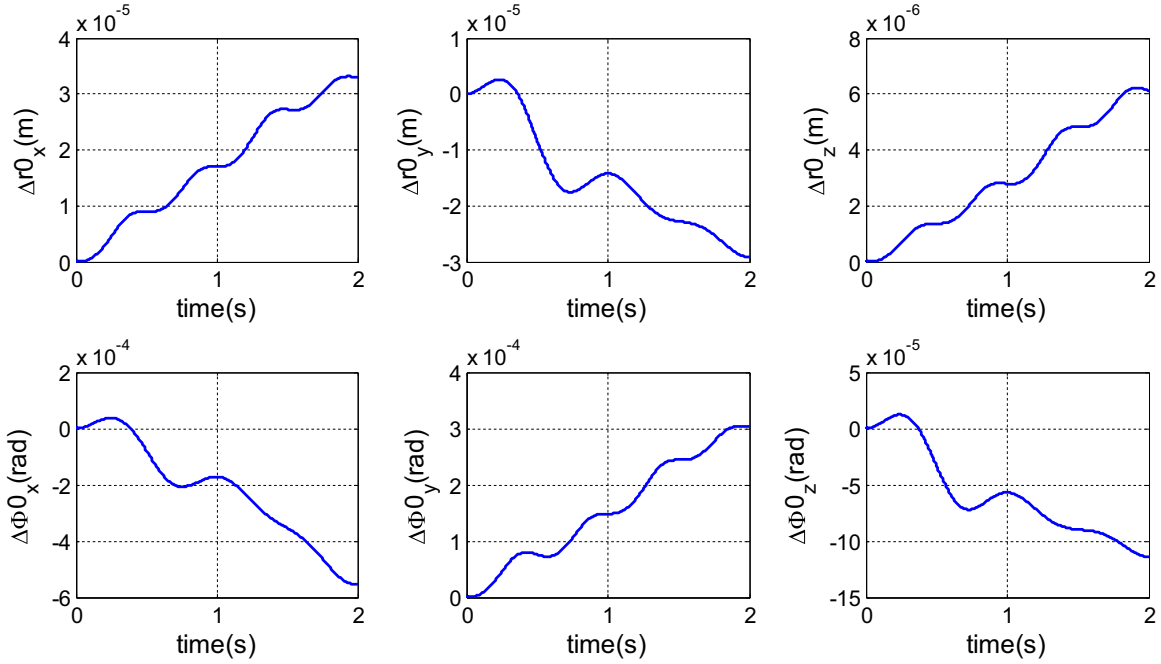

Fig. 12. Base's position error and attitude error of validation model.

of the base centroid position, base attitude and joint angles are respectively 3.31×10^{-5} m, -5.56×10^{-4} rad, and 7.96×10^{-4} rad. We can see that, the identified dynamic model are correct enough.

5.6. Sensitivity analysis of inertial parameters

Under ideal conditions, the linear and angular momentum equations of the equivalent two-body system are as follows:

$$\boldsymbol{P} = m_0\boldsymbol{v}_0 + m_1\boldsymbol{v}_1 = 0 \tag{63}$$

$$\boldsymbol{L} = (\boldsymbol{A}_0{}^0\boldsymbol{I}_0\boldsymbol{A}_0^{\mathrm{T}})\boldsymbol{\omega}_0 + (\boldsymbol{A}_1{}^1\boldsymbol{I}_1\boldsymbol{A}_1^{\mathrm{T}})\boldsymbol{\omega}_1 + \boldsymbol{r}_0\times(m_0\boldsymbol{v}_0) + \boldsymbol{r}_1\times(m_1\boldsymbol{v}_1) = 0 \tag{64}$$

If the identified parameters are inaccuracy, there will exist:

$$\hat{\boldsymbol{P}} = \hat{m}_0\boldsymbol{v}_0 + \hat{m}_1\boldsymbol{v}_1 \neq 0 \tag{65}$$

$$\hat{\boldsymbol{L}} = (\boldsymbol{A}_0{}^0\hat{\boldsymbol{I}}_0\boldsymbol{A}_0^{\mathrm{T}})\boldsymbol{\omega}_0 + (\boldsymbol{A}_1{}^1\hat{\boldsymbol{I}}_1\boldsymbol{A}_1^{\mathrm{T}})\boldsymbol{\omega}_1 + \hat{\boldsymbol{r}}_0\times(\hat{m}_0\boldsymbol{v}_0) + \hat{\boldsymbol{r}}_1\times(\hat{m}_1\boldsymbol{v}_1) \neq 0 \tag{66}$$

To analyze the sensitivity of the inertia parameters, we derive the partial derivative of the corresponding parameters. Expanding Eq. (63), the result is as follows:

$$\begin{bmatrix} P_x \\ P_y \\ P_z \end{bmatrix} = \begin{bmatrix} m_0v_{0x} + m_1v_{1x} \\ m_0v_{0y} + m_1v_{1y} \\ m_0v_{0z} + m_1v_{1z} \end{bmatrix} \tag{67}$$

Then, the sensitivity coefficient corresponding to the mass can be obtained by differentiating Eq. (67), i.e.:

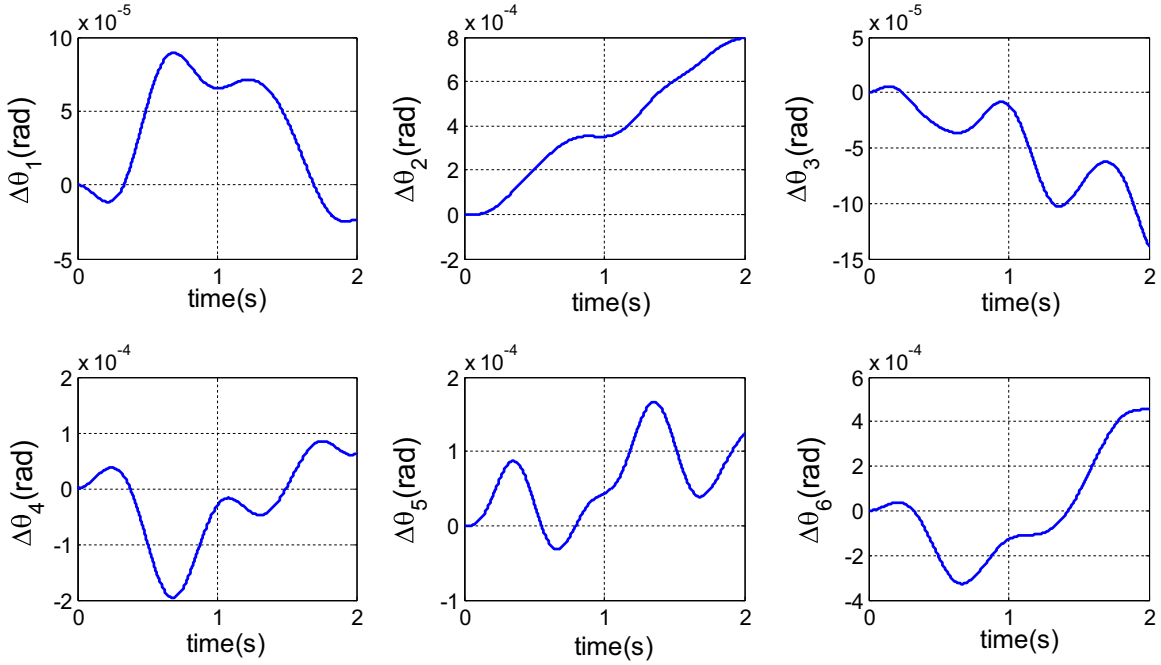

Fig. 13. Joint angle error of validation model ($\Delta q_1 \sim \Delta q_6$).

$$\begin{cases} \frac{\partial P_x}{\partial m_0} = v_{0x},\ \frac{\partial P_y}{\partial m_0} = v_{0y},\ \frac{\partial P_z}{\partial m_0} = v_{0z} \\ \frac{\partial P_x}{\partial m_1} = v_{1x},\quad \frac{\partial P_y}{\partial m_1} = v_{1y},\quad \frac{\partial P_z}{\partial m_1} = v_{1z} \end{cases} \tag{68}$$

That is to say, the error of m_i is dependent on the linear velocity values. According to Eq. (64), the matrix $\boldsymbol{A}_0$ can be set that:

$$\mathbf{A}_0 = \begin{bmatrix} a_{11} & a_{12} & a_{13} \\ a_{21} & a_{22} & a_{23} \\ a_{31} & a_{32} & a_{33} \end{bmatrix} \tag{69}$$

Substituting Eq. (69) into $(\boldsymbol{A}_0{}^0\boldsymbol{I}_0\boldsymbol{A}_0^{\mathrm{T}})\boldsymbol{\omega}_0$, we can obtain the following equations:

$$(\boldsymbol{A}_0{}^0\boldsymbol{I}_0\boldsymbol{A}_0^{\mathrm{T}})\boldsymbol{\omega}_0 = \begin{bmatrix} a_{11} & a_{12} & a_{13} \\ a_{21} & a_{22} & a_{23} \\ a_{31} & a_{32} & a_{33} \end{bmatrix} \begin{bmatrix} I_{0xx} & I_{0xy} & I_{0xz} \\ I_{0xy} & I_{0yy} & I_{0yz} \\ I_{0xz} & I_{0yz} & I_{0zz} \end{bmatrix} \begin{bmatrix} a_{11} & a_{21} & a_{31} \\ a_{12} & a_{22} & a_{32} \\ a_{13} & a_{23} & a_{33} \end{bmatrix} \begin{bmatrix} \omega_{0x} \\ \omega_{0y} \\ \omega_{0z} \end{bmatrix} \tag{70}$$

Then, Eq. (70) can be simplified as:

$$(\boldsymbol{A}_0{}^0\boldsymbol{I}_0\boldsymbol{A}_0^{\mathrm{T}})\boldsymbol{\omega}_0 = \begin{bmatrix} K_1 I_{0xx} + K_2 I_{0xy} + K_3 I_{0xz} + K_4 I_{0yy} + K_5 I_{0yz} + K_6 I_{0zz} \\ K_7 I_{0xx} + K_8 I_{0xy} + K_9 I_{0xz} + K_{10} I_{0yy} + K_{11} I_{0yz} + K_{12} I_{0zz} \\ K_{13} I_{0xx} + K_{14} I_{0xy} + K_{15} I_{0xz} + K_{16} I_{0yy} + K_{17} I_{0yz} + K_{18} I_{0zz} \end{bmatrix} \tag{71}$$

where,

$$\begin{cases} K_1 = a_{11}S_1,\ K_2 = a_{12}S_1 + a_{11}S_2,\ K_3 = a_{13}S_1 + a_{11}S_3 \\ K_4 = a_{12}S_2,\ K_5 = a_{13}S_2 + a_{12}S_3,\ K_6 = a_{13}S_3 \\ K_7 = a_{21}S_1,\ K_8 = a_{22}S_1 + a_{21}S_2,\ K_9 = a_{23}S_1 + a_{21}S_3 \\ K_{10} = a_{22}S_2,\ K_{11} = a_{23}S_2 + a_{22}S_3,\ K_{12} = a_{23}S_3 \\ K_{13} = a_{31}S_1,\ K_{14} = a_{32}S_1 + a_{31}S_2,\ K_{15} = a_{33}S_1 + a_{31}S_3 \\ K_{16} = a_{32}S_2,\ K_{17} = a_{33}S_2 + a_{32}S_3,\ K_{18} = a_{33}S_3 \\ S_1 = \omega_{0x}a_{11} + \omega_{0y}a_{21} + \omega_{0z}a_{31} \\ S_2 = \omega_{0x}a_{12} + \omega_{0y}a_{22} + \omega_{0z}a_{32} \\ S_3 = \omega_{0x}a_{13} + \omega_{0y}a_{23} + \omega_{0z}a_{33} \end{cases} \tag{72}$$

Then, the sensitivity coefficient of inertia tensor can be obtained by differentiating Eq. (64), i.e.:

$$\begin{cases} \frac{\partial L_x}{I_{0xx}} = K_1,\ \frac{\partial L_x}{I_{0xy}} = K_2,\ \frac{\partial L_x}{I_{0xz}} = K_3,\ \frac{\partial L_x}{I_{0yy}} = K_4,\ \frac{\partial L_x}{I_{0yz}} = K_5,\ \frac{\partial L_x}{I_{0zz}} = K_6 \\ \frac{\partial L_y}{I_{0xx}} = K_7,\ \frac{\partial L_y}{I_{0xy}} = K_8,\ \frac{\partial L_y}{I_{0xz}} = K_9,\ \frac{\partial L_y}{I_{0yy}} = K_{10},\ \frac{\partial L_y}{I_{0yz}} = K_{11},\ \frac{\partial L_y}{I_{0zz}} = K_{12} \\ \frac{\partial L_z}{I_{0xx}} = K_{13},\ \frac{\partial L_z}{I_{0xy}} = K_{14},\ \frac{\partial L_z}{I_{0xz}} = K_{15},\ \frac{\partial L_z}{I_{0yy}} = K_{16},\ \frac{\partial L_z}{I_{0yz}} = K_{17},\ \frac{\partial L_z}{I_{0zz}} = K_{18} \end{cases} \tag{73}$$

Assuming the maximum angular velocity of $\mathrm{B}_{\mathbf{0}}$ is 0.03 rad/s, so we can obtain that:

$$\|S_i\| \le 0.03, \qquad (i = 1, 2, 3) \tag{74}$$

Then, the sensitivity coefficient will meet the following constraints, i.e.:

$$\begin{cases} \|K_i\| \le 0.03, \quad (i = 1, 4, 6, 7, 10, 12, 13, 16, 18) \\ \|K_i\| \le 0.06 \quad (i = 2, 3, 5, 8, 9, 11, 14, 15, 17) \end{cases} \tag{75}$$

Similarly, the sensitivity of B_1's parameters can be analyzed. Based on the analysis, we can evaluate the range of the accuracy, determine the identification strategy and plan appropriate movement path.

6. Conclusion

Inertia parameters are very important in controlling space robots with a high degree of accuracy. This paper proposes a practical and effective method for identifying the complete inertia parameters of space robotic system. The identification of the whole system is decomposed into the identification of equivalent single- and two-body systems. For the former, all of the joints are locked into the normal configuration and the thrusters are used for orbital maneuvering. The object function is defined in terms of acceleration and velocity. For the latter, only one joint is unlocked and driven to move along a planned (exiting) trajectory under the base in free-floating mode. Linear and angular momentum conservation are used to define the object function. Therefore, the parameter identification problem is transformed into a non-linear optimization problem, and the parameters are determined using the PSO algorithm. The proposed method is very easy but effective, and can be extended to many other cases, such as:

1) If all of the inertia parameters in all of the bodies must be identified, then orbital maneuvering and acceleration measurement must be required to identify an equivalent single-body system.
2) If the mass and centroid position of any system body (such as the base) are known, then only the attitude maneuvering of the equivalent single-body system is required to identify the inertia tensor.
3) If the inertia parameters of the base or manipulator are known, then only the equivalent two-body system needs to be identified. The parameters of other bodies are easily determined according to the momentum conservation. The orbital maneuvering and acceleration measurement are not required.
4) Based on the known or identified parameters of the space robot, the grasped target can easily be identified using the equivalent two-body system identification concept.
5) Other than the first case, in which all of the inertia parameters of all of the bodies must be identified, orbital maneuvering and acceleration measurement is not required; only velocity measurement is required. Then the fuel is not consumed, and the method is not affected by internal forces.

Acknowledgements

This work was supported in part by the National Natural Science Foundation of China (61573116), and the Basic Research Program of Shenzhen (JCYJ20160427183553203 and JCYJ 20150529141408781).

References

[1] A. Flores-Abad, O. Ma, K. Pham, S. Ulrich, A review of space robotics technologies for on-orbit servicing, Prog. Aerosp. Sci. 68 (2014) 1–26.
[2] F. Aghili, A prediction and motion-planning scheme for visually guided robotic capturing of free-floating tumbling objects with uncertain dynamics, IEEE Trans. Robot. 28 (3) (2012) 634–649.
[3] L. Felicetti, P. Gasbarri, A. Pisculli, M. Sabatini, G.B. Palmerini, Design of robotic manipulators for orbit removal of spent launchers's stages, Acta Astronaut. 119 (2016) 118–130.
[4] P. Huang, B. Liu, Fan Zhang, Configuration maintaining control of three-body ring tethered system based on thrust compensation, Acta Astronaut. 123 (2016) 37–50.
[5] D. Wang, P. Huang, Z. Meng, Coordinated stabilization of tumbling targets using tethered space manipulators, IEEE Trans. Aerosp. Electron. Syst. 51 (3) (2015) 2420–2432.
[6] K. Nanos, E. Papadopoulos, Avoiding dynamic singularities in cartesian motions of free-floating manipulators, IEEE Trans. Aerosp. Electron. Syst. 51 (3) (2015) 2305–2318.
[7] W. Xu, D. Meng, Y. Chen, H. Qian, Y. Xu, Dynamics modeling and analysis of a flexible-base space robot for capturing large flexible spacecraft, Multibody Syst. Dyn. 32 (3) (2014) 357–401.
[8] Y. Umetani, K. Yoshida, Resolved motion rate control of space manipulators with generalized jacobian matrix, IEEE Trans. Robot. Autom. 5 (3) (1989) 303–314.
[9] Y. Nakamura, R. Mukherjee, Nonholonomic path planning of space robots via a bidirectional approach, IEEE Trans. Robot. Autom. 7 (4) (1991) 500–514.
[10] D.N. Nenchev, K. Yoshida, P. Vichitkulsawat, M. Uchiyama, Reaction null-space control of flexible structure mounted manipulator systems, IEEE Trans. Robot. Autom. 15 (6) (1999) 1011–1023.
[11] K.Yoshida, K.Hashizume, S.Abiko, Zero reaction maneuver: flight validation with ETS-VII space robot and extension to kinematically redundant arm, in: Proceedings IEEE International Conference on Robotics and Automation, Piscataway, USA, 2001, pp. 441–446.
[12] W. Xu, C. Li, X. Wang, B. Liang, Y. Liu, Y. Xu, Study on non-holonomic cartesian path planning of free-floating space robotic system, Adv. Robot. 23 (1–2) (2009) 113–143.
[13] M. Oda, Y. Ohkami, Coordination control of spacecraft attitude and space manipulators, Control Eng. Pract. 5 (1) (1997) 11–21.
[14] A. Flores-Abad, Z. Wei, O. Ma, K. Pham, Optimal control of space robots for capturing a tumbling object with uncertainties, J. Guid. Control Dyn. 37 (6) (2014)

2014–2017.
[15] G. Dong, Z.H. Zhu, Position-based visual servo control of autonomous robotic manipulators, Acta Astronaut. 115 (2015) 291–302.
[16] B.P. Larouche, Z.H. Zhu, Autonomous robotic capture of non-cooperative target using visual servoing and motion predictive control, Auton. Robots 37 (2) (2014) 157–167.
[17] Y. Murotsu, K. Senda, M. Ozaki, Parameter identification of unknown object handled by free-flying space robot, J. Guid. Control Dyn. 17 (3) (1994) 488–494.
[18] K.Yoshida, S.Abiko, Inertia parameter identification for a free-flying space robot, in: Proceedings AIAA Guidance, Navigation, and Control Conference and Exhibit, Monterey, California, USA, 2002, pp. 1–8.
[19] R.Lampariello, G.Hirzinger, Modeling and experimental design for the on-orbit inertial parameter identification of free-flying space robots, in: Proceedings IDETC/CIE 2005 ASME 2005 International Design Engineering Technical Conferences and Computers and Information in Engineering Conference, Long Beach, California, USA, 2005, pp. 1–10.
[20] S.Abiko, G.Hirzinger, On-line parameter adaptation for a momentum control in the post-grasping of a tumbling target with model uncertainty, in: Proceedings IEEE/RSJ International Conference on Intelligent Robots and Systems, San Diego, CA, USA, 2007, pp. 847–852.
[21] O. Ma, H. Dang, On-orbit identification of inertia properties of spacecraft using a robotic arm, J. Guid. Control Dyn. 31 (6) (2008) 1761–1771.
[22] T. Nguyen-Huynh, I. Sharf, Adaptive reactionless motion and parameter identification in postcapture of space debris, J. Guid. Control Dyn. 36 (2) (2013) 404–414.
[23] S. Dubowsky, E. Papadopoulos, The kinematics, dynamics, and control of free-flying and free-floating space robotic systems, IEEE Trans. Robot. Autom. 9 (5) (1993) 531–543.
[24] H. Wang, Y. Xie, Prediction error based adaptive jacobian tracking for free-floating space manipulators, IEEE Trans. Aerosp. Electron. Syst. 48 (4) (2012) 3207–3221.
[25] R. Poli, J. Kennedy, T. Blackwell, Particle swarm optimization, Swarm Intell. 1 (1) (2007) 33–57.